Major facilitator superfamily domain-containing protein 10 (MFSD10)

A Target Enabling Package (TEP)

Gene ID / UniProt ID	**10227** / **Q14728**
Target Nominator	CMD Internal Nomination
Authors	Tomas C. Pascoa[1], Ashley C.W. Pike[1], Simon R. Bushell[1], Andrew Quigley[1], Shubhashish M.M. Mukhopadhyay[1], Nicola A. Burgess-Brown[1], Elisabeth P. Carpenter[1].
Target PI	Liz Carpenter / Alex Bullock (CMD Oxford)
Therapeutic Area(s)	Inflammation
Disease Relevance	MFSD10 mediates efflux of non-steroidal anti-inflammatory drugs such as indomethacin and diclofenac.
Date Approved by TEP Evaluation Group	2nd June 2021
Document version	1.0
Document version date	July 2021
Citation	Tomas C. Pascoa, Ashley C.W. Pike, Simon R. Bushell, Andrew Quigley, Shubhashish M.M. Mukhopadhyay, Nicola A. Burgess-Brown, & Elisabeth P. Carpenter. (2021). Major facilitator superfamily domain-containing protein 10 (MFSD10) A Target Enabling Package (TEP) [Data set]. Zenodo. http://doi.org/10.5281/zenodo.5126783
Affiliations	[1] Centre for Medicine Discovery, University of Oxford, Old Road Campus Research Building, Headington, Oxford OX3 7DQ.

USEFUL LINKS

(Please note that the inclusion of links to external sites should not be taken as an endorsement of that site by the SGC in any way)

SUMMARY OF PROJECT

MFSD10 (also known as TETRAN in humans) has been proposed to function as an organic anion efflux pump and as a transporter for some NSAIDs. We have produced milligram quantities of purified recombinant protein and solved its structure in an outward-facing state at 2.6 Å resolution by X-ray crystallography. The structure - the first example for a human atypical SLC - provides the initial clues to understanding the broad specificity of its putative substrate-binding site.

SCIENTIFIC BACKGROUND

Non-steroidal anti-inflammatory drugs (NSAIDs) are one of the most widely prescribed classes of drugs and exert their anti-inflammatory effects by blocking prostaglandin biosynthesis via inhibition of the

cyclooxygenases COX-1 and/or COX-2 (**Fig 1A**). Pharmaceutical inhibition of the COX enzymes can provide relief from the symptoms of inflammation and pain. However, NSAID use can give rise to a range of gastrointestinal, cardiovascular and renal complications.

MFSD10 (also known as TETRAN in humans) was first identified nearly thirty years ago through its similarity to the *E. coli* tetracycline drug-resistant transporters (e.g. TetA(B)) but its substrates remained unknown (1). Over a decade later, over-expression of MFSD10 was found to confer resistance to apoptosis induced by NSAIDs in a human adenocarcinoma gastric cell line (2) (**Fig 1B**). Moreover, NSAID sensitivity was restored by siRNA-knockdown of MFSD10 expression leading to MFSD10's proposed role as an NSAID efflux pump (**Fig 1C**). Subsequent studies have shown that MFSD10, which is expressed at high levels in the heart, kidney and prostate, can mediate transport of some but not all NSAIDs (3). More recently, MFSD10 has been found to be enriched in the nuclear envelope and could be implicated in transporting toxic metabolites and/or xenobiotics across the inner nuclear membrane into the ER lumen (4). Nonetheless, MFSD10's subcellular localisation remains unclear.

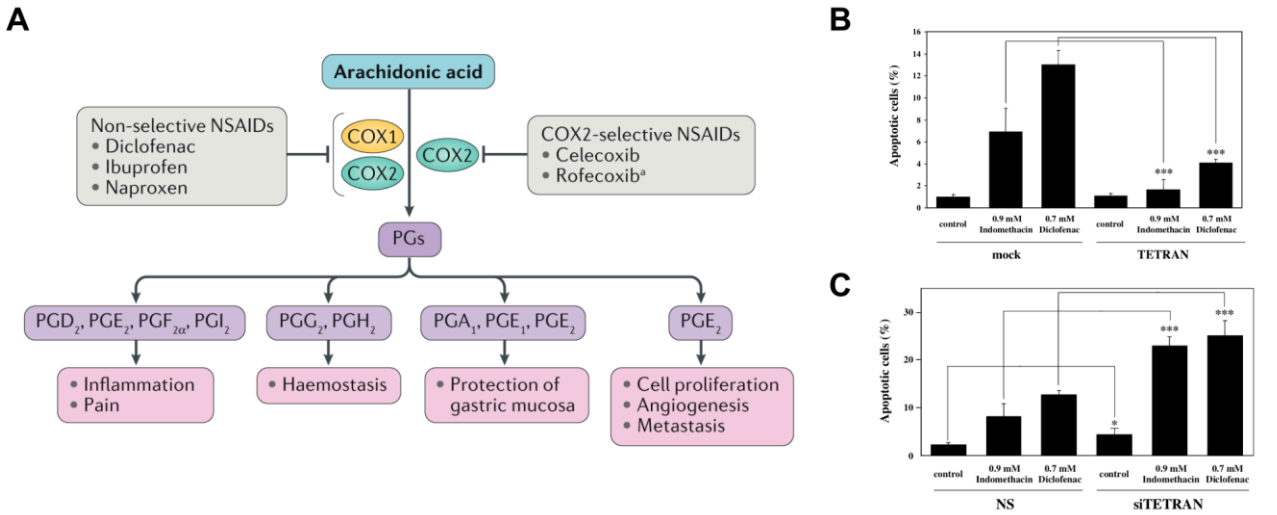

Figure 1. (A) NSAIDs inhibit the cyclooxygenase(COX)-catalysed conversion of arachidonic acid to prostaglandins (Figure reproduced from Schjerning *et al* (2020) (5). (B) MFSD10 over-expression confers resistance to NSAID-mediated apoptosis. (C) MFSD10 siRNA knockdown enhances NSAID-mediated apoptosis. Panels B and C reproduced from Fig6c and Fig7b in Mima *et al*. 2007 (2).

MFSD10 belongs to the major facilitator superfamily (MFS) that are found in all kingdoms of life and includes transporters for the export and import of target substrates. MFS transporters are secondary active transporters that operate through an alternate access mechanism where conformational changes in the transmembrane (TM) helices enable a centrally located substrate-binding site to be alternately accessible from either side of the membrane (6,7). MFS transporters, of which there are 129 in humans, are the largest family in the solute carrier (SLC) superfamily of membrane transport proteins. MFSD10 has low sequence similarity to other members of the solute carrier (SLC) families and is classified as an atypical SLC, assigned to atypical MFS transporter family 1 (AMTF1), as it could not be placed within any of the existing SLC families based on sequence identity alone. More recent sequence and phylogenetic analysis suggest the AMTF1 could be placed within the SLC46 family (8,9).

Approximately 30% of solute carriers are classified as orphans having unknown function, expression profile and substrate specificity. In this TEP, we have developed methods for protein expression and purification of MFSD10 as well as solving its structure, as a first step towards de-orphanisation of this target. Our data provide the first molecular insight into how organic anions bind to this atypical SLC.

RESULTS – THE TEP

Proteins purified

Human MFSD10 is 455 amino acids in length and predicted to have twelve transmembrane (TM) segments. We have expressed a C-terminally truncated construct of MFSD10 (Met1-Lys444) with a C-terminal TEV-10His-Flag tag in insect (*Sf9*) cells. MFSD10 is isolated and purified in octyl glucose neopentyl glycol (OGNG) supplemented with cholesteryl hemisuccinate (CHS) at yields of between 0.3 - 0.8 mg purified protein / litre culture. Purified MFSD10 can be concentrated up to 40 mg/ml in this detergent/lipid combination.

Structural data

We have crystallised MFSD10 using the lipidic cubic phase (LCP) method and solved its structure to a resolution of 2.6 Å [PDB: **6S4M**]. Overall MFSD10 has 12 TM helices (TM1-TM12) which adopt a canonical MFS fold (**Fig 1**). The TM helices are arranged as two 6TM bundles (TM1-6 & TM7-12) connected by an intracellular linker region (ICH1-3) that is partially embedded in the membrane bilayer (**Fig 1A,B**).

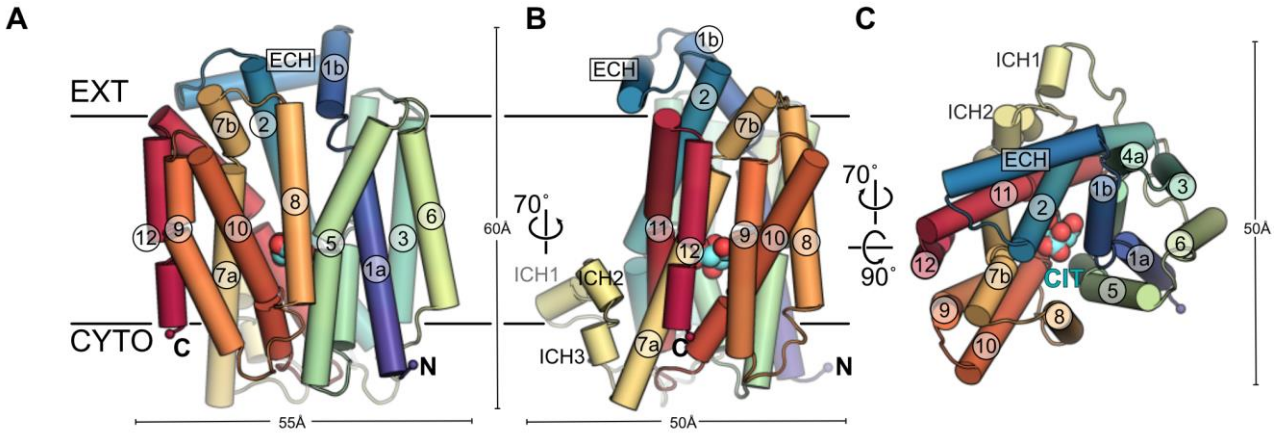

Figure 1. Structure of human MFSD10 [PDB: 6S4M] viewed (A,B) from the membrane plane and (C) from the extracellular face. The bound citrate anion (cyan/red) is shown in space-filling form.

In the crystals, MFSD10 is captured in an outward-facing, partially-occluded conformation (**Fig 2AB**). The central cavity, with a depth of 35 Å, is lined by TM1a/b, TM2, TM4a/b and TM5 from the N-terminal bundle and TM7a/b, TM8, TM10 and TM11 from the C-terminal bundle. The extracellular gate, formed by TM1-2 and TM7-8 is partially open to the extracellular side with a narrow slot-shaped entrance, 7.5 Å x 18 Å wide, leading to a larger solvent-filled cavity. The intracellular gate, composed of TM4-5 and TM10-11 is closed, preventing access to the central cavity from the cytoplasm.

A putative substrate binding site lies at the bottom of the open cavity and is predominantly lined by residues from TM5, TM7a, TM10 and TM11 (**Fig 2C,D**). The binding site has a distinct charged/non-polar character with a polar pocket between TM7 and TM11 and a more hydrophobic face contributed by TM4 and TM5 (**Fig 2D**). There is some unexplained residual difference electron density in the substrate-binding site adjacent to Tyr279 (TM7a), Arg401 and Arg408 (TM11) that can be nicely accounted for by a citrate molecule derived from the crystallization solution (**Fig 2C,D**). The citrate anion nestles at the bottom end of the outward open central cavity at a depth of about 24 Å from the extracellular entrance. One of its terminal carboxylate groups binds adjacent to Tyr279 and also hydrogen bonds to both arginines on TM11 (Arg401 / Arg408). The other two carboxylate groups interact with either Arg401 or Arg408 (**Fig 2C**). The citrate anion also makes non-polar contacts with Val157 (TM4), Phe184 (TM5), Leu283 (TM7a) Val377 (TM10), Gly404 (TM11).

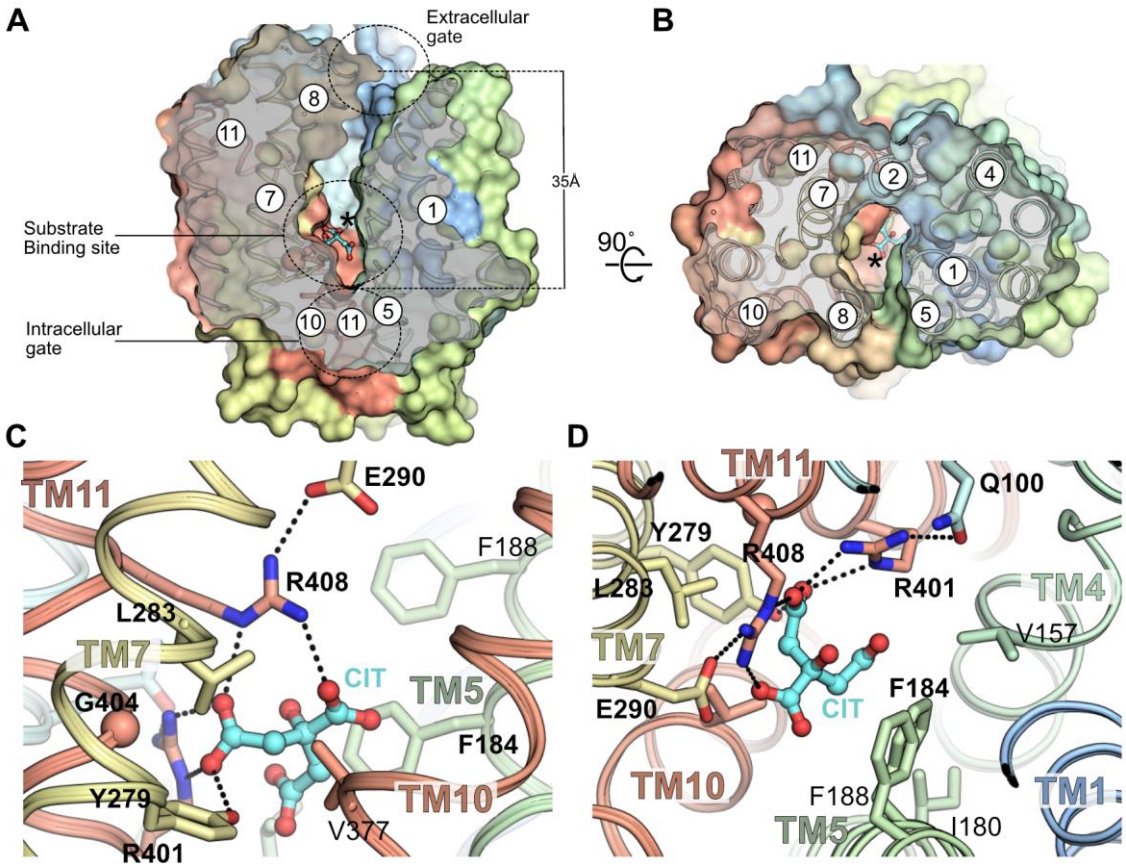

Figure 2. **(A,B)** Cutaway molecular surface showing partially occluded substrate binding cavity. Structure is viewed in **(A)** the same orientation as Fig. 1A and in **(B)** as in Fig. 1C. Citrate in stick representation is indicated by asterisk. **(C-D)** Detailed view of interactions with citrate molecule (*cyan*) in 'substrate' binding site viewed from **(C)** parallel to the membrane plane, **(D)** from the extracellular side of the membrane looking towards the cytoplasm. TM helices are coloured as in Fig. 1. Dotted lines in C and D indicate hydrogen bonds.

The binding mode of the citrate anion sheds light on the likely interaction of NSAIDs such as diclofenac and indomethacin with MFSD10. These NSAIDs have slightly anionic properties with an acidic group that, like the citrate carboxylate, most probably binds in the TM7/TM11 polar pocket. The remainder of the NSAID scaffold is variable but typically possesses a hydrophobic character that could be accommodated by the more hydrophobic TM4/5 face of the substrate binding site that lies adjacent to the carboxylate binding site (**Fig 3**).

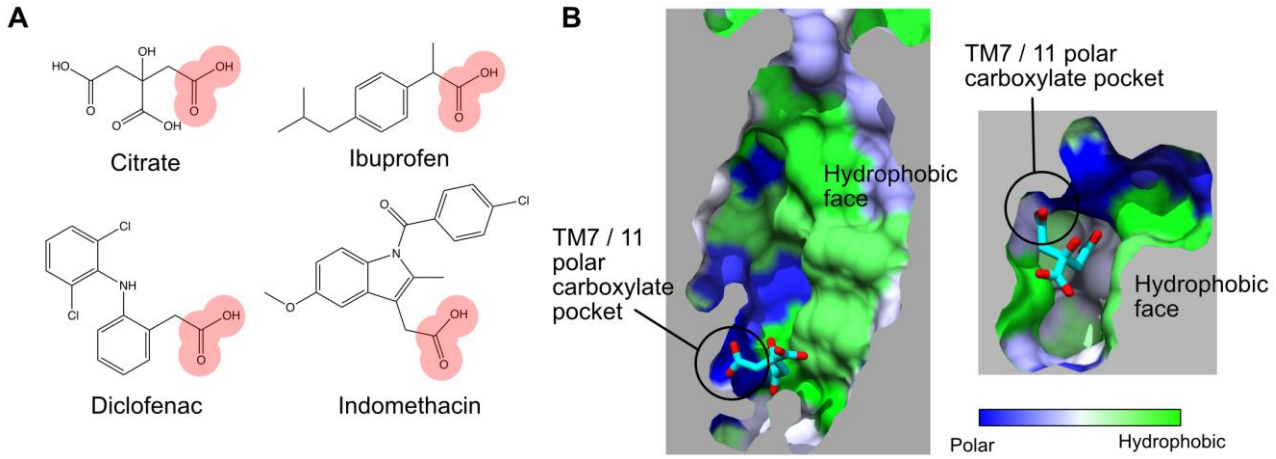

Figure 3. **(A)** Molecular stuctures of organic anions. **(B)** Substrate binding site. Molecular surface is coloured by the Kyte-Doolittle amino acid hydrophobicity index with least hydrophobic in blue and most hydrophobic in green. Binding pocket is viewed parallel to membrane plane (*left*) and from the extracellular face (*right*).

A previous study revealed that NSAID transport by MFSD10 is sensitive to nigericin, a H^+/K^+ exchanger, suggesting it is coupled to the proton motive force (3). In addition, MFSD10 contains a conserved sequence "antiporter" motif (Motif C), which is present in MFS antiporters, but not found in uniporters or symporters (10). In MFSD10, this sequence motif is ^{178}**A**VIGVAFSL**G**FTL**GP**ML**GA**^{196} and is located on TM5 which forms part of the hydrophobic face of the substrate binding cavity. Together the available evidence suggested that MFSD10 could act as a proton-coupled antiporter, using the inwardly directed H^+ electrochemical gradient to drive the conformational change to the inward-facing state, where it can bind another substrate molecule. Using a pyranine-based assay (*see next section*) we demonstrate that NSAID application results in proton translocation. Glu290 is the most likely titratable residue present in the central cavity. Glu290 is located on TM7a and is solvent accessible from the extracellular environment. In our outward-facing structure it forms a salt-bridge with Arg408 in TM11 and its close proximity may preclude protonation (**Fig 2C**). Since MFS antiporters typically couple substrate release to protonation and because Arg408 appears to form an integral part of the substrate binding-site, displacement of the Arg408 side chain upon substrate release could act as the trigger for protonation of Glu290.

Assays

We have demonstrated that MFSD10 reconstituted into proteoliposomes acts as an NSAID/H^+ exchanger (**Fig 4**). This was achieved by directly monitoring proton movement during the transport cycle using a pyranine-based assay. Pyranine is a ratiometric pH-sensitive dye which can be encapsulated into proteoliposomes and used to track changes in their internal pH (11). By alternately exciting pyranine at 415nm and 460nm while monitoring fluorescence at 510nm, the ratio of fluorescence emission upon excitation at 460nm/415nm increases with increasing pH. Using this experimental setup, we observed that application of external diclofenac results in alkalinisation of the lumen (**Fig 4BC**). Control experiments (without MFSD10 protein) show that the recorded increase in internal pH is a direct result of substrate transport by MFSD10. In summary, this method has enabled us to monitor the coupled proton flux and confirmed that MFSD10 acts as an NSAID/H+ antiporter.

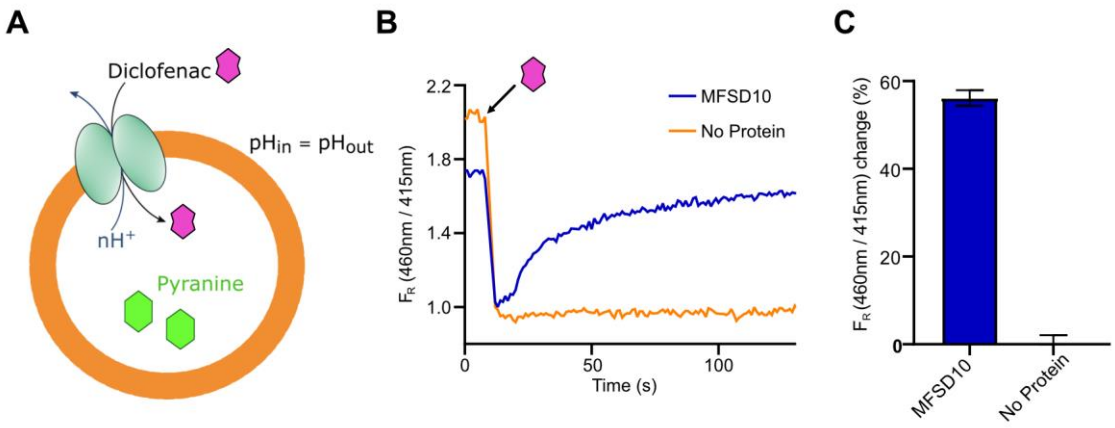

Figure. 4. Pyranine based assay to demonstrate MFSD10-dependent, NSAID/H^+ antiport. **(A)** Schematic representation of the experimental setup for diclofenac-driven proton flux experiments. MFSD10 (light green ovals) was reconstituted into liposomes (orange ring), which were then loaded with the pH-sensitive dye pyranine (green polygon). Addition of diclofenac (2mM; magenta polygon) drives proton efflux from the liposomes. This results in alkalinisation of the liposome lumen, which alters pyranine fluorescence. **(B)** MFSD10 activity monitored using this experimental setup. Pyranine fluorescence was monitored (emission 510nm; excitation 460nm and 415nm) and the F_R (ratio of fluorescence at 510nm when excited at 460nm/415nm) is plotted. Addition of 2mM diclofenac (marked by an arrow/magenta polygon), causes an initial drop in F_R and subsequently leads to alkalinisation of MFSD10-containing proteoliposomes (observed as an increase in F_R; blue trace). In control liposomes without protein, F_R remains unchanged after the initial drop caused by diclofenac interference (orange trace). **(C)** Bar chart showing the relative change in F_R in MFSD10 proteoliposomes and control liposomes without protein. Data shown are the average from triplicate experiments; error bars correspond to the standard error of the mean.

Future plans

MFSD10 has been nominated as a priority target in the pan-European ReSOLUTE consortium, in which the CMD participates in, that has the overall aim of enhancing our knowledge of all SLC transporters and evaluating their tractability as drug targets (12). In terms of MFSD10, the immediate goal is to provide tools to assist in target de-orphanisation. To this end, we are providing our recombinant MFSD10 protein to consortium members for nanobody generation (Saša Štefanić, Nanobody Service Facility (NSF), University of Zurich) and SURFE^{2}R assay development (ReSOLUTE pharma partner).

CONCLUSION

NSAID efflux may represent a protective mechanism to counteract the adverse effects of this class of widely used drugs and MFSD10 has been demonstrated to confer resistance to NSAID-mediated apoptosis. However, the underlying mechanism is uncharacterized, in part due to lack of recombinant proteins, validated protein binders and biophysical / structural data.

To address this gap, we have solved the first structure of the human organic anion efflux transporter MFSD10 in an outward facing, partially occluded state. A fortuitous co-crystallised organic anion provides some clues to molecular determinants of substrate recognition. We also provide methodology for the robust expression, purification and reconstitution of MFSD10 into proteoliposomes for further functional evaluation.

TEP IMPACT

Publications arising from this work:

To be published: Tomas C. Pascoa, Ashley C.W. Pike, Simon R. Bushell, Andrew Quigley, Amy Chu, Shubhashish M.M. Mukhopadhyay, Leela Shrestha, Nicola Burgess-Brown, Elizabeth P. Carpenter. '*Crystal structure of the atypical human NSAID/H+ antiporter MFSD10*' in preparation.

FUNDING INFORMATION

The work performed at the SGC has been funded by a grant from the Wellcome [106169/ZZ14/Z].

ADDITIONAL INFORMATION

Structure Files

PDB ID	Structure Details
6S4M	MFSD10 / TETRAN crystal structure in outward facing state

Materials and Methods

Protein Expression and Purification

Vector: pFB-CT10HF-LIC (available from The Addgene Nonprofit Plasmid Repository)

Cell line: DH10Bac, Sf9 cells

Tags and additions: C-terminal TEV protease site, followed by 10x His and FLAG tags

Construct sequence: Residues 1 – 444

MGWGGGGGCTPRPPIHQQPPERRVVTVVFLGLLLDLLAFTLLLPLLPGLLESHGRAHDPLYGSWQGGVDWFATAIGMPVE
KRYNSVLFGGLIGSAFSVLQFLCAPLTGATSDCLGRRPVMLLCLMGVATSYAVWATSRSFAAFLASRLIGGISKGNVSLSTAIV
ADLGSPLARSQGMAVIGVAFSLGFTLGPMLGASLPLEMAPWFALLFAASDLLFIFCFLPETLPLEKRAPSIALGFRDAADLLSPL
ALLRFSAVARGQDPPSGDRLSSLRRLGLVYFLYLFLFSGLEYTLSFLTHQRFQFSSLQQGKMFFLIGLTMATIQGAYARRIHPGG
EVAAVKRALLLLVPAFLLIGWGRSLPVLGLGLLLYSFAAAVVVPCLSSVVAGYGSPGQKGTVMGTLRSLGALARAAGPLVAAS
VYWLAGAQACFTTWSGLFLLPFFLLQKAENLYFQSHHHHHHHHHHDYKDDDDK

(underlined sequence contains vector encoded TEV protease cleavage site, His and FLAG tag)

Expression

The human MFSD10 gene (HGNC: 16894; Gene ID 10227), which encodes the MFSD10/TETRAN protein (Major facilitator superfamily protein 10; residues Met1 to Lys444), was subcloned into the pFB-CT10HF-LIC vector and baculovirus was generated using the Bac-to-Bac system. Briefly, this was performed by transforming into the *Escherichia co*li strain DH10Bac, to generate bacmid DNA, which was then used to transfect *Spodoptera frugiperda* (Sf9) insect cells, from which recombinant baculovirus were obtained. Large scale grow-ups of Sf9 cells (2 x 10^6 cells / mL) were infected with baculovirus (5 mL / L) and incubated for 72 h at 27 °C in 2 L roller bottles. Cells were harvested by centrifugation at 900 g for 10 min. The cell pellets were resuspended in PBS and pelleted again by centrifugation at 900 g for 20 min, then flash-frozen in liquid nitrogen and stored at -80 °C.

Cell Lysis and detergent extraction of membrane proteins

Extraction Buffer (EXB): 50 mM HEPES-NaOH, pH 7.5, 200 mM NaCl, Roche protease inhibitor cocktail EDTA-free (1 tablet was used for 40 ml resuspended cells, dissolved in 1 ml Extraction buffer per tablet by vortexing prior to addition to the cell pellets).

Cell pellets were resuspended in EXB buffer at the ratio of 50 ml per litre of equivalent original cell culture. The resuspension was then passed twice through an EmulsiFlex-C5 homogenizer (Avestin Inc.) at 15000 psi. Membrane proteins were extracted from the cell lysate with 1% w/v octyl glucose neopentyl glycol (OGNG; Generon, Cat. No. NG311) / 0.1% cholesteryl hemisuccinate tris salt (CHS; Sigma-Aldrich, Cat. No. C6512) and rotated for 1 h at 4 °C. Cell debris was removed by centrifugation at 35,000 x *g* for 1 h at 4 °C.

Purification

Wash Buffer: 50 mM HEPES-NaOH, pH 7.5, 200 mM NaCl, 0.12% w/v OGNG / 0.012% w/v CHS and 20 mM imidazole pH 8.0

Elution Buffer: 50 mM HEPES-NaOH, pH 7.5, 200 mM NaCl, 0.12% w/v OGNG / 0.012% w/v CHS and 250 mM imidazole pH 8.0

PD10 Buffer: 50 mM HEPES-NaOH, pH 7.5, 200 mM NaCl, 0.12% w/v OGNG / 0.012% w/v CHS

Size exclusion buffer (SEC) Buffer: 20 mM HEPES-NaOH, pH 7.5, 200 mM NaCl, 0.12% w/v OGNG/ 0.012% w/v CHS

Column 1: Co2+ TALON resin

The detergent-extracted supernatant was supplemented with 5 mM imidazole pH 8.0 before incubation with Co^{2+} charged TALON resin (Clontech) for 2 h on a rotator at 4 °C (1.5 ml resin slurry per L original culture volume). The Talon resin was collected by centrifugation at 700 x *g* for 5 mins and washed with 30 column volumes of wash buffer before the target protein was eluted with elution buffer. Peak fractions were combined and passed through PD10 columns, pre-equilibrated with five column volumes of PD10 buffer.

TEV protease cleavage and reverse purification

TEV protease was added at a ratio of 10:1 (MFSD10:enzyme, wt:wt) and incubated at 4 °C overnight. For each litre of initial cell culture volume, 0.4 ml of a 50% slurry of TALON resin (pre-equilibrated as above) was added and the sample was rotated at 4 °C for 1 hour. The sample was transferred to a gravity column and the flow-through was collected.

Column 2: Superdex 200 Increase 10/300 GL column (GE Healthcare)

The protein sample was concentrated in a 100 kDa MWCO Vivaspin 20 centrifugal concentrator (pre-equilibrated in SEC buffer without detergent) at 3,000 g, with mixing every 5 min, to a final volume of ca. 0.5 ml. After centrifugation at 21,000 g for 20 min at 4^{o} C, the sample was subjected to size exclusion chromatography

Crystallisation

Initial protein crystals were grown in lipidic cubic phase (LCP) sandwich plates at 20 °C in an in-house PEG400/Salt Screen (0.1 M ADA pH 6.5, 0.2 M lithium citrate, 30 % v/v polyethylene glycol (PEG) 400) in 96-well glass sandwich plates (Paul Marienfeld, Germany). 50 nL of LCP bolus were dispensed and overlaid with 800nl solution using a Mosquito LCP robot (TTP Labtech). Crystals appeared after 1-2 days and grew to full size within 1 week. Crystals were vitrified in liquid nitrogen directly from the drop using MiTeGen dual thickness MicroMounts. Diffraction data were collected at the I24 microfocus beamline at Diamond Light Source.

Structure Determination

MFSD10 crystallises in monoclinic space group $P2_1$ with a single copy of the transporter in each asymmetric unit. Diffraction data were mildly anisotropic and limited to between 3.1 Å resolution in the worse direction and 2.4 Å in the best direction. Initial phase estimates were obtained using PHASER (13) with the coordinates of YajR (PDB: 3WDO)(14) as a search model. A density-modified map was used to generate an initial model with BUCCANEER (15). Model completion was carried out manually in COOT (16) and the structure was refined with REFMAC using all data to 2.4 Å. The final model comprises residues 18-443, two monoolein molecules and 60 solvent molecules.

Reconstitution of MFSD10 into proteoliposomes

Lipids obtained as 25mg/mL stocks in chloroform (Avanti Polar Lipids) were combined in a round-bottomed flask (3:1 (w:w) POPE:POPG) and the chloroform was evaporated using a rotary evaporator to obtain a thin lipid film. The lipids were then re-suspended in SEC buffer without detergent, sonicated, and subjected to 5 freeze-thaw cycles to form large multilamellar vesicles (LMVs). LMVs were then extruded 21x through a 400nm polycarbonate filter (Avestin) to yield large unilamellar vesicles (LUVs) which were then disrupted with 0.15% (w:v) Triton X-100 (determined to enable membrane saturation with detergent by monitoring OD_{540}). Purified protein was added at 1:50 (w:w) protein:lipid and the mixture was incubated for 30 minutes at 4^{o}C. Triton X-100 was then removed through the sequential addition of Bio-Beads^{TM} SM-2 (Biorad). Proteoliposomes were collected by ultracentrifugation (1 hour at 100,000 x g), resuspended in the desired buffer, flash frozen in liquid N_2, and stored at -80^{o}C.

Pyranine assay

Proteoliposomes were prepared as described above, resuspended in Inside Buffer (5mM HEPES pH 6.8, 119mM NaCl, 1mM KCl, 2mM $MgSO_4$) supplemented with 1mM pyranine, and subjected to three freeze-thaw cycles. Proteoliposomes were then extruded 21x through a 400nm followed by a 200nm polycarbonate filters (Avestin), and unincorporated pyranine was removed using Bio-Spin 6 columns (Biorad). For the assay, desalted proteoliposomes were diluted 1:25 into Outside Buffer (5mM HEPES pH 7.5, 119mM NaCl, 1mM KCl, 2mM MgSO4) and a baseline was recorded by monitoring emission at 510nm while alternating the excitation wavelength between 460nm and 415nm. Transport was initiated with 2mM diclofenac and fluorescence was monitored for 2 minutes post-injection. Liposomes without protein were included as a control. Fluorescence measurements were carried out in a 96-well plate format on a Clariostar plate reader (BMG Labtech) and the results analysed with Prism (Graphpad).

References

1. Duyao, M. P., Taylor, S. A. M., Buckler, A. J., Ambrose, C. M., Lin, C., Groot, N., Church, D., Barnes, G., Wasmuth, J. J., Housman, D. E., Macdonald, M. E., and Gusella, J. F. (1993) A gene from chromosome 4p 16.3 with similarity to a superfamily of transporter proteins. *Human Molecular Genetics* **2**, 673-676

2. Mima, S., Ushijima, H., Hwang, H.-J., Tsutsumi, S., Makise, M., Yamaguchi, Y., Tsuchiya, T., Mizushima, H., and Mizushima, T. (2007) Identification of the TPO1 gene in yeast, and its human orthologue TETRAN, which cause resistance to NSAIDs. **581**, 1457-1463
3. Ushijima, H., Hiasa, M., Namba, T., Hwang, H. J., Hoshino, T., Mima, S., Tsuchiya, T., Moriyama, Y., and Mizushima, T. (2008) Expression and function of TETRAN, a new type of membrane transporter. *Biochem Biophys Res Commun* **374**, 325-330
4. Cheng, L.-C., Baboo, S., Lindsay, C., Brusman, L., Martinez-Bartolomé, S., Tapia, O., Zhang, X., Yates, J. R., and Gerace, L. (2019) Identification of new transmembrane proteins concentrated at the nuclear envelope using organellar proteomics of mesenchymal cells. *Nucleus* **10**, 126-143
5. Schjerning, A.-M., McGettigan, P., and Gislason, G. (2020) Cardiovascular effects and safety of (non-aspirin) NSAIDs. *Nature Reviews Cardiology* **17**, 574-584
6. Jardetzky, O. (1966) Simple allosteric model for membrane pumps. *Nature* **211**, 969-970
7. Drew, D., North, R. A., Nagarathinam, K., and Tanabe, M. (2021) Structures and General Transport Mechanisms by the Major Facilitator Superfamily (MFS). *Chem Rev*
8. Sreedharan, S., Stephansson, O., Schiöth, H. B., and Fredriksson, R. (2011) Long evolutionary conservation and considerable tissue specificity of several atypical solute carrier transporters. *Gene* **478**, 11-18
9. Perland, E., Bagchi, S., Klaesson, A., and Fredriksson, R. (2017) Characteristics of 29 novel atypical solute carriers of major facilitator superfamily type: evolutionary conservation, predicted structure and neuronal co-expression. *Open Biology* **7**, 170142
10. Varela, M. F., Sansom, C. E., and Griffith, J. K. (1995) Mutational analysis and molecular modelling of an amino acid sequence motif conserved in antiporters but not symporters in a transporter superfamily. *Molecular Membrane Biology* **12**, 313-319
11. Kano, K., and Fendler, J. H. (1978) Pyranine as a sensitive pH probe for liposome interiors and surfaces. pH gradients across phospholipid vesicles. *Biochim Biophys Acta* **509**, 289-299
12. Superti-Furga, G., Lackner, D., Wiedmer, T., Ingles-Prieto, A., Barbosa, B., Girardi, E., Goldmann, U., Gurtl, B., Klavins, K., Klimek, C., Lindinger, S., Lineiro-Retes, E., Muller, A. C., Onstein, S., Redinger, G., Reil, D., Sedlyarov, V., Wolf, G., Crawford, M., Everley, R., Hepworth, D., Liu, S., Noell, S., Piotrowski, M., Stanton, R., Zhang, H., Corallino, S., Faedo, A., Insidioso, M., Maresca, G., Redaelli, L., Sassone, F., Scarabottolo, L., Stucchi, M., Tarroni, P., Tremolada, S., Batoulis, H., Becker, A., Bender, E., Chang, Y. N., Ehrmann, A., Muller-Fahrnow, A., Putter, V., Zindel, D., Hamilton, B., Lenter, M., Santacruz, D., Viollet, C., Whitehurst, C., Johnsson, K., Leippe, P., Baumgarten, B., Chang, L., Ibig, Y., Pfeifer, M., Reinhardt, J., Schonbett, J., Selzer, P., Seuwen, K., Bettembourg, C., Biton, B., Czech, J., de Foucauld, H., Didier, M., Licher, T., Mikol, V., Pommereau, A., Puech, F., Yaligara, V., Edwards, A., Bongers, B. J., Heitman, L. H., AP, I. J., Sijben, H. J., van Westen, G. J. P., Grixti, J., Kell, D. B., Mughal, F., Swainston, N., Wright-Muelas, M., Bohstedt, T., Burgess-Brown, N., Carpenter, L., Durr, K., Hansen, J., Scacioc, A., Banci, G., Colas, C., Digles, D., Ecker, G., Fuzi, B., Gamsjager, V., Grandits, M., Martini, R., Troger, F., Altermatt, P., Doucerain, C., Durrenberger, F., Manolova, V., Steck, A. L., Sundstrom, H., Wilhelm, M., and Steppan, C. M. (2020) The RESOLUTE consortium: unlocking SLC transporters for drug discovery. *Nat Rev Drug Discov* **19**, 429-430
13. McCoy, A. J., Grosse-Kunstleve, R. W., Adams, P. D., Winn, M. D., Storoni, L. C., and Read, R. J. (2007) Phaser crystallographic software. *Journal of Applied Crystallography* **40**, 658-674
14. Jiang, D., Zhao, Y., Wang, X., Fan, J., Heng, J., Liu, X., Feng, W., Kang, X., Huang, B., Liu, J., and Zhang, X. C. (2013) Structure of the YajR transporter suggests a transport mechanism based on the conserved motif A. *Proceedings of the National Academy of Sciences of the United States of America* **110**, 14664-14669
15. Cowtan, K. (2006) The Buccaneer software for automated model building. 1. Tracing protein chains. *Acta Crystallographica Section D: Biological Crystallography* **62**, 1002-1011
16. Emsley, P., Lohkamp, B., Scott, W. G., and Cowtan, K. (2010) Features and development of Coot. *Acta crystallographica. Section D, Biological crystallography* **66**, 486-501

We respectfully request that this document is cited using the DOI value as given above if the content is used in your work.